Solution-based adaptive parallel patterning by laser-induced local plasmonic surface defunctionalization

Bongchul Kang, Jongsu Kim, and Minyang Yang*

Department of Mechanical Engineering, Korea Advanced Institute of Science and Technology (KAIST), Daejeon, 305-701, South Korea

myyang@kaist.ac.kr

Abstract: Adaptive mass fabrication method based on laser-induced plasmonic local surface defunctionalization was suggested to realize solution-based high resolution self-patterning on transparent substrate in parallel. After non-patterned functional monolayer was locally deactivated by laser-induced metallic plasma species, various micro/nano metal structures could be simultaneously fabricated by the parallel self-selective deposition of metal nanoparticles on a specific region. This method makes the eco-friendly and cost-effective production of high resolution pattern possible. Moreover, it can respond to design change actively due to the broad controllable range and easy change of key patterning specifications such as a resolution (subwavelength~100 μm), thickness (100 nm~6 μm), type (dot and line), and shape.

OCIS codes: (140.3390) Laser materials processing; (160.4236) Nanomaterials; (220.4000) Microstructure fabrication; (310.1860) Deposition and fabrication; (310.6628) Subwavelength structures, nanostructures; (350.5400) Plasmas.

References and links

1. Z. Bao, Y. Feng, A. Dodabalapur, V. R. Raju, and A. J. Lovinger, "High-performance plastic transistors fabricated by printing techniques," Chem. Mater. **9**(6), 1299–1301 (1997).
2. C. W. Sele, T. von Werne, R. H. Friend, and H. Sirringhaus, "Lithography-free, self-aligned inkjet printing with sub-hundred-nanometer resolution," Adv. Mater. (Deerfield Beach Fla.) **17**(8), 997–1001 (2005).
3. B. Kang, S. Ko, J. Kim, and M. Yang, "Microelectrode fabrication by laser direct curing of tiny nanoparticle self-generated from organometallic ink," Opt. Express **19**(3), 2573–2579 (2011).
4. D. Pile, "Organic electronics: laser-induced electrode fabrication," Nat. Photonics **5**(4), 199 (2011).
5. B. Kang, S. Han, J. Kim, S. Ko, and M. Yang, "One-step fabrication of copper electrode by laser-induced direct local reduction and agglomeration of copper oxide nanoparticle," J. Phys. Chem. C **115**(48), 23664–23670 (2011).
6. B. Kang, J. Kno, and M. Yang, "High-resolution and high-conductive electrode fabrication on a low thermal resistance flexible substrate," J. Micromech. Microeng. **21**(7), 075017 (2011).
7. A. Bonito, M. Picasso, and M. Laso, "Numerical simulation of 3D viscoelastic flows with free surfaces," J. Comput. Phys. **215**(2), 691–716 (2006).
8. F. C. Krebs, "Roll-to-roll fabrication of monolithic large-area polymer solar cells free from indium-tin-oxide," Sol. Energy Mater. Sol. Cells **93**(9), 1636–1641 (2009).
9. T. C. M. Sotomayor, *Alternative Lithography.* (Springer: NewYork, 2003).
10. S. H. Ko, I. Park, H. Pan, C. P. Grigoropoulos, A. P. Pisano, C. K. Luscombe, and J. M. J. Fréchet, "Direct nanoimprinting of metal nanoparticles for nanoscale electronics fabrication," Nano Lett. **7**(7), 1869–1877 (2007).
11. J. C. Love, L. A. Estroff, J. K. Kriebel, R. G. Nuzzo, and G. M. Whitesides, "Self-assembled monolayers of thiolates on metals as a form of nanotechnology," Chem. Rev. **105**(4), 1103–1170 (2005).
12. R. K. Smith, P. A. Lewis, and P. S. Weiss, "Patterning self-assembled monolayers," Prog. Surf. Sci. **75**(1-2), 1–68 (2004).
13. M. H. Lin, C. F. Chen, H. W. Shiu, C. H. Chen, and S. Gwo, "Multilength-scale chemical patterning of self-assembled monolayers by spatially controlled plasma exposure: nanometer to centimeter range," J. Am. Chem. Soc. **131**(31), 10984–10991 (2009).
14. W. Chang, M. Choi, J. Kim, S. Cho, and K. Whang, "Sub-micron scale patterning using femtosecond laser and self-assembled monolayers interaction," Appl. Surf. Sci. **240**(1-4), 296–304 (2005).

#175246 - $15.00 USD Received 30 Aug 2012; revised 5 Oct 2012; accepted 16 Oct 2012; published 14 Dec 2012

15. Y. Zhang, R. H. Terrill, T. A. Tanzer, and P. W. Bohn, "Ozonolysis is the primary cause of UV photooxidation of alkanethiolate monolayers at Low Irradiance," J. Am. Chem. Soc. **120**(11), 2654–2655 (1998).
16. D. J. Kim, J. M. Lee, J. G. Park, and B. G. Chung, "A self-assembled monolayer-based micropatterned array for controlling cell adhesion and protein adsorption," Biotechnol. Bioeng. **108**(5), 1194–1202 (2011).
17. Y. X. Zhuang, O. Hansen, T. Knieling, C. Wang, P. Rombach, W. Lang, W. Benecke, M. Kehlenbeck, and J. Koblitz, "Thermal stability of vapor phase deposited self-assembled monolayers for MEMS anti-stiction," J. Micromech. Microeng. **16**(11), 2259–2264 (2006).
18. K. Neil, Adam, *The Physics and Chemistry of Surfaces,* 3rd ed. (Oxford University Press, 1941).
19. W. Zhou, J. Zhang, Y. Liu, X. Li, X. Niu, Z. Song, G. Min, Y. Wan, L. Shi, and S. Feng, "Characterization of anti-adhesive self-assembled monolayer for nanoimprint lithography," Appl. Surf. Sci. **255**(5), 2885–2889 (2008).
20. R. Noll, R. Sattmann, V. Sturm, and S. Winkelmann, "Space- and time-resolved dynamics of plasmas generated by laser double pulses interacting with metallic samples," J. Anal. At. Spectrom. **19**(4), 419–428 (2004).
21. H. R. Pakhal, R. P. Lucht, and N. M. Laurendeau, "Spectral measurements of incipient plasma temperature and electron number density during laser ablation of aluminum in air," Appl. Phys. B **90**(1), 15–27 (2008).
22. S. S. Harilal, M. S. Tillack, B. O'Shay, C. V. Bindhu, and F. Najmabadi, "Confinement and dynamics of laser-produced plasma expanding across a transverse magnetic field," Phys. Rev. E Stat. Nonlin. Soft Matter Phys. **69**(2), 026413 (2004).
23. B. Wu, Y. C. Shin, H. Pakhal, N. M. Laurendeau, and R. P. Lucht, "Modeling and experimental verification of plasmas induced by high-power nanosecond laser-aluminum interactions in air," Phys. Rev. E Stat. Nonlin. Soft Matter Phys. **76**(2 Pt 2), 026405 (2007).
24. B. Wu, "High-intensity nanosecond-pulsed laser-induced plasma in air, water, and vacuum: A comparative study of the early-stage evolution using a physics-based predictive model," Appl. Phys. Lett. **93**(10), 101104 (2008).
25. X. L. Liu, X. Lu, X. Liu, T. T. Xi, F. Liu, J. L. Ma, and J. Zhang, "Tightly focused femtosecond laser pulse in air: from filamentation to breakdown," Opt. Express **18**(25), 26007–26017 (2010).
26. S. H. Ko, Y. Choi, D. J. Hwang, C. P. Grigoropoulos, J. Chung, and D. Poulikakos, "Nanosecond laser ablation of gold nanoparticle films," Appl. Phys. Lett. **89**(14), 141126 (2006).
27. J. Chung, S. Ko, N. R. Bieri, C. P. Grigoropoulos, and D. Poulikakos, "Conductor microstructures by laser curing of printed gold nanoparticle ink," Appl. Phys. Lett. **84**(5), 801–803 (2004).
28. H. W. Fox and W. A. Zisman, "The spreading of liquids on low energy surfaces. I. polytetrafluoroethylene," J. Colloid Sci. **5**(6), 514–531 (1950).
29. B. Medasani, Y. H. Park, and I. Vasiliev, "Theoretical study of the surface energy, stress, and lattice contraction of silver nanoparticles," Phys. Rev. B **75**(23), 235436 (2007).
30. H. Y. Ko, J. Park, H. Shin, and J. Moon, "Rapid self-assembly of monodisperse colloidal spheres in an ink-jet printed droplet," Chem. Mater. **16**(22), 4212–4215 (2004).

1. Introduction

Recently, electronic industries are faced with a new challenge developing low-cost, simple and flexible fabrication process according to the rapidly changing market needs. Until now, photolithography and vacuum deposition process have been usually used to fabricate the high resolution metal pattern that is a main component of electronics. Although these methods are useful for making the high quality micro features in parallel, these require a high processing temperature, many fabrication steps, multiple vacuum processes and toxic chemicals. Furthermore, it is almost impossible to change the design of the expensive templates such as photo and shadow mask once it is fabricated.

As a low-cost mask-free fabrication method alternative to the conventional photolithography processes, various ink-jet printing methods based on metal nanoparticle (NP) solution were demonstrated. But the achievable minimum resolution is limited to 30~50 μm due to the nonlinear dispensing and nozzle size limitation [1,2]. Laser direct curing (LDC) of NPs was suggested to improve the resolution and uniformity for large area [3–6]. However, there are some critical problems, for example, the limitation of patterning speed (~1 mm/s) by a series of NPs sintering; expansive ultrafine NP below 5 nm required for productivity and conductivity; thickness limit by laser penetration depth; large material consumption by washing of unwanted region [3–6]. Most importantly, these serial processes are not suitable for mass production since the production time linearly increases with the fabrication area and pattern density. As a parallel patterning method to enhance productivity, various roll printing methods based on a physically engraved mold were developed. But, in most cases, the minimum resolution is limited to approximately 20 μm [7,8]. Besides, as an alternative maskless lithography method, imprinting lithography was developed to fabricate two-dimensional structures with submicrometer resolution. Its major advantages are low-cost,

#175246 - $15.00 USD Received 30 Aug 2012; revised 5 Oct 2012; accepted 16 Oct 2012; published 14 Dec 2012

high-throughput production of various nanostructures with operational ease. However, imprinting lithography for metals is typically an indirect process due to their high melting temperature where a polymer (e.g., UV-curable polymers and poly(methyl methacrylate)PMMA) pattern is first created by imprinting, which is then used as mask for dry etching of a pre-deposited metal film or as part of the metal lift-off process [9]. So, conventional metal imprinting lithography involves multiple steps and expensive processes, thereby increasing the cost of manufacturing and offsetting the advantages of the imprinting process. Although the direct imprinting process of NPs was recently developed to simply realize sub-micron feature patterning [10], these parallel methods accompany the sacrifice of process flexibility and require the huge initial investment due to a need of expensive master mold fabricated by conventional photolithography.

A self-assembled monolayer (SAM) was being regarded as a good functional surface to deposit solutions selectively due to the distinct wetting property depending on a surface energy [11,12]. Although the chemical surface mold based on SAM has great merits of low cost and short time for the mold fabrication due to the elimination of a step making the physically engraved mold, template based complicate processes such as O_2 plasma or ultraviolet light treatment using mask and contact printing using polydimethylsiloxane (PDMS) mold were needed to selectively form the SAM on transparent substrate [11–13]. Although direct writing based SAM patterning methods using laser was already attempted to photo-thermally or photo-chemically deactivate the SAM deposited on light absorbable substrates such as a gold film and silicon [11,14,15], it was not applied for a transparent substrate that is useful for display/optical devices, due to the limited light absorption [14,15]. Therefore, there is an intense need of the development of laser based template-free patterning process of SAM coated on a transparent substrate for a solution processable high resolution pattern fabrication combining the high process flexibility of serial processes and high productivity of parallel processes.

In this study, we newly suggested a low-cost adaptive mass fabrication method based on laser-induced plasmonic local surface-defunctionalization in order to realize solution processable high resolution self-patterning on transparent substrate. A SAM coated on the overall surface of a substrate was permanently deactivated by the momentary laser-induced local plasma derived by the physical interaction of a laser and thin metal film deposited on SAM, as shown in Fig. 1(a). The silver (Ag) NP solution with polarity was self-selectively deposited only on the laser processed surface by simply dip-coating the solution on the processed substrate, as shown in Fig. 1(b). Finally, the micro/nano Ag conductive structure could be easily fabricated through the simple sintering process of the dip-coated substrate. This approach has obvious advantages compared to conventional photolithography and other maskless fabrication methods. First, the outstanding process flexibility is achievable because the resolution, shape, type, and thickness of pattern could be easily controlled by changing some processing conditions. Next, the overall productivity can be more improved than that of conventional parallel processes since any expensive templates, chemical etching process, and complicate fabrication steps are not required by the high speed defunctionalization and parallel direct self-patterning in vacuum-free environment. Lastly, it is eco-friendly and low-cost process due to the waste-free deposition of material and absence of harmful etchants.

2. Experiment

The soda lime glass of 1 mm thickness was used as a transparent substrate in this study. The used Ag NP of was supported by ABC Nanotech Co. The average particle size is approximately 20 nm, as shown the transmission electron microscope (TEM) image in Fig. 1(b). The Ag NPs was dispersed into propylene glycol monomethyl ether (PGME), a kind of polar solvents, for dewetting on a hydrophobic surface. Finally, the Ag NP solution with an Ag weight ratio of 30%, a surface tension of 33 mN/m and a viscosity of 5.7 cp was synthesized. The contact angle of the prepared Ag NP solution for a bare glass was recorded as approximately 0 ° by a contact angle meter (DSA100 from Krűss GmbH). To modify the hydrophilic surface of a bare glass into hydrophobic one, the tridecafluoro-1,1,2,2-

#175246 - $15.00 USD Received 30 Aug 2012; revised 5 Oct 2012; accepted 16 Oct 2012; published 14 Dec 2012

tetrahydrooctyltrichlorosilane (FOTS, $CF_3(CF_2)_5(CH_2)_2SiCl_3$) self-assembled monolayer (SAM), a kind of trifunctional silanes of CF_3 terminal group, was prepared due to its large contact angle above 100 ° for the water and good thermal stability above 400 °C [16,17]. And only trifunctional silanes are able to form monolayers which are strongly linked together by Si-O-Si-bonds [17]. Before the actual coating process, a glass substrate was immersed in piranha solution (1:3, H_2O_2:H_2SO_4) at 80 °C for 30 min and followed by quick dump rinse in DI water and smooth nitrogen brush drying at low temperature. The FOTS diluted by anhydrous toluene that is used as a carrier, was evaporated in a vacuum chamber of 0.2 mbar in order to uniformly deposit it on glass surface without the polymerization of FOTS by moisture in the air, as shown in Fig. 2(a) [17]. After the substrate had been removed from chamber, it was rinsed with toluene (twice), ethanol (twice), and DI water (twice) to remove any physisorbed material. The contact angle of the prepared Ag NP solution on FOTS coated glass was measured as being 55 °. In preliminary experiments, it was determined that more large contact angle was required to enhance the wetting selectivity of the solution. So, the solution cooled by 4 °C was used to increase its own surface tension as well as decrease the vapor pressure [18]. Finally, the more increased contact angle of 63.5 ° than that in ambient temperature have been achieved, as shown in Fig. 2(b).

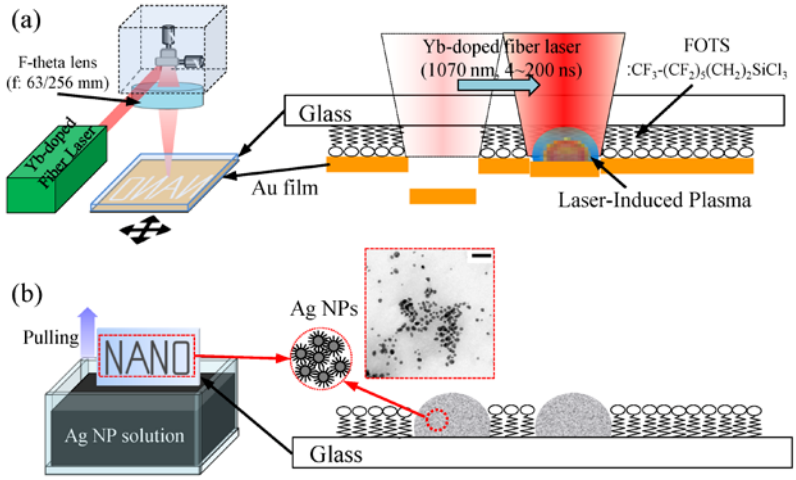

Fig. 1. Schematics of proposed process: (a) Experimental setup and selective defuctionalization by laser induced plasma. (b) Self-patterning of Ag NPs on selective defunctionalized substrate by immersion. The inset is TEM image of Ag NPs (scale = 100 nm).

Thin gold (Au) film with a thickness of 50 nm was deposited on the SAM coated surface using an e-beam evaporation. Here, a gold that is chemically stable for CF_3 silane was selected as a metal layer to induce the plasma because the chemical bonding between the deposited metal layer and SAM should be avoided to be easy to detach the metal layer after laser irradiation [19]. The ns-pulsed ytterbium-doped fiber laser with 1070 nm wavelength, which can adjust a laser pulse width (W_p) in discrete steps was employed as an energy source to generate the plasma. The laser beam passed through the glass substrate from the front side and was absorbed on an Au layer on the rear surface. As a result, the metallic plasma was simultaneously generated at the interface between the SAM and Au layer, as shown in Fig. 1(a). The plasma is commonly generated by the instantaneous energy interaction between incident laser and gas evaporated by metal ablation, which contains high energetic species such as ions, radicals and electrons [20–22]. The laser beam spot with a 10/25 μm focal diameter ($1/e^2$) was controlled by an x-y galvanometer scanner and two kinds of f-theta lens with 63 and 256 mm focal lengths. After laser processing, the residual Au layer in the unexposed region was peeled off from the glass substrate using a conventional scotch tape.

#175246 - $15.00 USD Received 30 Aug 2012; revised 5 Oct 2012; accepted 16 Oct 2012; published 14 Dec 2012

The Ag solution was selectively deposited on the fabricated specimen through immersing and withdrawing it in Ag NP solution.

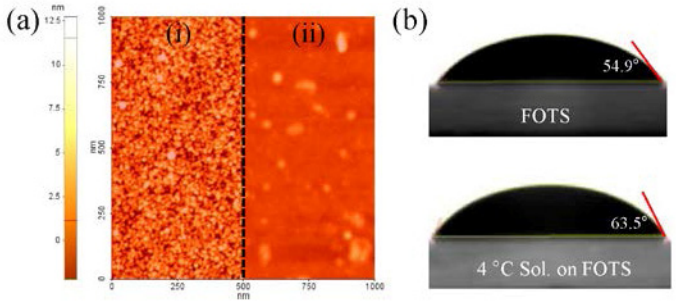

Fig. 2. (a) Atomic force microscope image of (i) liquid phase deposited SAM and (ii) vacuum phase deposited one. (b) Contact angle of Ag nanopraticle solution in the ambient temperature and 4 °C on FOTS.

3. Results and discussion

As a method to investigate the interaction between the laser induced plasma and SAM, the focused laser was irradiated onto the opposite side of SAM coated surface in the condition without the spatial overlap between laser pulses at 200 ns pulse width, 60 μJ pulse energy, 2 kHz pulse repetition rate (PRR), and 250 mm/s scan rate. It was observed that the glass surface on the laser-irradiated region was damaged, as shown in Fig. 3(a). Although the interaction mechanism of the SAM by the laser-induced plasma is considered to be either the contribution of energetic species in the plasma or the plasma heating at the front of plasma plume [23,24]. From the damage appearance shown in Fig. 3(a), it is judged that the thermal damages such as crack occurrence and melting came from the high temperature (above 10^4 K) of the plasma front and strong shock wave by plasma generated at interface between the glass surface and gold layer. So, it is considered that the deactivation of SAM in this experiment was due to the instantaneously thermal decomposition [17]. To relieve this physical damage of glass surface, the laser pulse energy decreased to 30 μJ. Moreover, the pulse width of irradiated laser was varied to 50, 100 and 200 ns in order to investigate the effect of the temporal overlap between the incident laser pulse and generated plasma. The laser-induced plasma could be highly affected by a laser pulse width since the plasma generated by the complicate interaction between a laser pulse and metal layer is occurred within the plasma delay time of several tens nanoseconds [22–24]. Figure 3(b) shows the microscopic images of partially self-patterned solution on the laser processed glass in the condition of a laser spot size of 25 μm, a pulse width of 200, 100, and 50 ns, a pulse energy of 30 μJ, a PRR of 2 kHz and a scanning rate of 170 mm/s after dip-coating it in the Ag NP solution. In the results of a pulse width of 200 and 100 ns, the thermal damage on laser irradiated surface was also occurred, as shown in Figs. 3(b)-3(i), 3(ii). Otherwise, in the results of a pulse width of 50 ns, the any thermal damages were not observed in microscopic measurement (Figs. 3(b)-3(iii)). This result indicates that only SAM layer could be deactivated by the laser-induced plasma without any defects and damages on substrate. Another notable point in these results is that the drop size of selectively wetted solution gradationally decreases with decreasing the pulse width from 200 ns to 50 ns, as shown in Fig. 3(b). Although the peak intensity of laser pulse relatively decreases with increasing in a pulse width, the interaction time between the generated plasma and incident laser pulse increases. So, the plasma can be spatially more grown and enhanced by the laser absorption of the generated plasma in the condition of relatively long pulse width [21]. So, the plasma treated area in the SAM can be laterally expanded by this interactional growth of plasma. For this reason, the selectively deposited solution in the condition of a pulse width of 50 ns appeared the smallest size among these

#175246 - $15.00 USD Received 30 Aug 2012; revised 5 Oct 2012; accepted 16 Oct 2012; published 14 Dec 2012

three pulse width conditions. Finally, it is concluded that the pulse width is the most dominant factor to affect the selectivity, resolution and thermal damage of substrate.

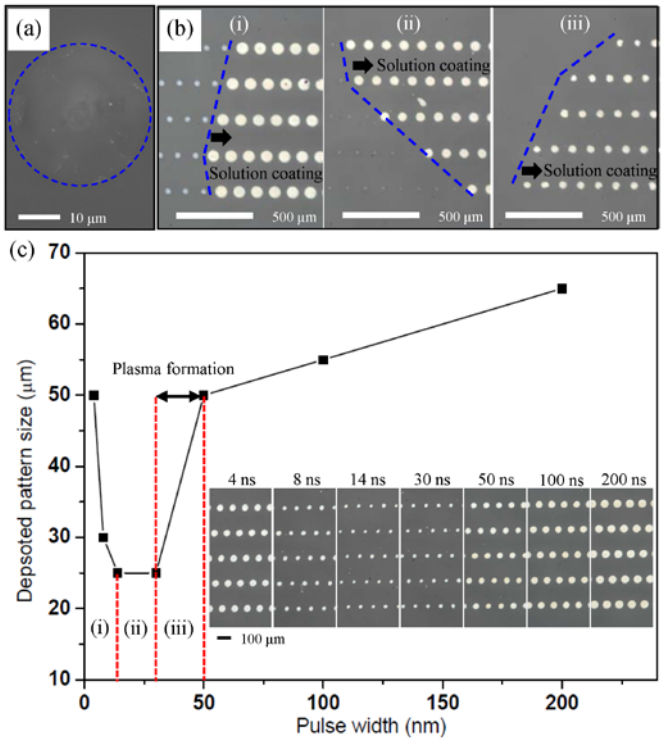

Fig. 3. (a) SEM image of defunctionalized substrate processed at 200 ns pulse width, 60 μJ pulse energy, 2 kHz repetition rate, and 250 mm/s scan rate. (b) Microscopic images of defunctionalized substrate partially immersed in Ag NPs at a pulse width of 30 μJ and a laser pulse width of (i) 200 ns, (ii) 100 ns, and (iii) 50 ns. (c) Size variation of self-deposited dot pattern with laser pulse width. The inset is corresponding microscope images.

To find the optimal pulse width condition more specifically, the pulse width of irradiated laser was varied more finely and shorter within the possible range to operate laser pulse, for example, 4, 8, 14, 30 and 50 ns. As shown in Fig. 3(c), the size of deposited solution gradually decreases with decreasing the pulse width from 200 ns until 30 ns (Figs. 3(c)-3(iii)), but the size rather starts to increase from a pulse width of 14 ns to 4 ns (Figs. 3(c)-3(i)). It is inferred that the broadening of solution wetted area and the occurrence of thermally damaged area on glass surface in short pulse width conditions below 14 ns mean the thermal interaction by excessive increase of laser peak power. Because the excessive decrease of pulse width leads to the sharp increase of laser peak power, the SAM can be thermally decomposed by the laser absorption of metal layer in spite of the absence of the interactional plasma growth occurred in a pulse width more than 30 ns (Figs. 3(c)-3(iii)) [14,15,23]. Therefore, the plasma growth/enhancement could be minimized in the condition of a pulse width of 14~30 ns (Figs. 3(c)-3(ii)) under a fixed laser pulse of 30 μJ since the size of wetted solution is almost similar with the laser spot and the thermal damage is not occurred, as shown in Fig. 3(c). It was determined that 14 ns is an optimized pulse width considering pattern resolution. Another important thing found in Fig. 3(c) is that it is possible to estimate plasma delay time approximately right after irradiating a laser pulse. In this experiment, it could be guessed that the plasma was formed in the region within 30~50 ns after irradiating a laser pulse on gold. If the laser pulse width is varied more finely in a step of 1 ns, the more specific plasma formation time could be found quantitatively. This approach will be used for low-cost indirect

#175246 - $15.00 USD Received 30 Aug 2012; revised 5 Oct 2012; accepted 16 Oct 2012; published 14 Dec 2012

method to measure the plasma delay time for various materials alternative to conventional expensive and complicate measurement method such as time-resolved shadowgraph [23,25].

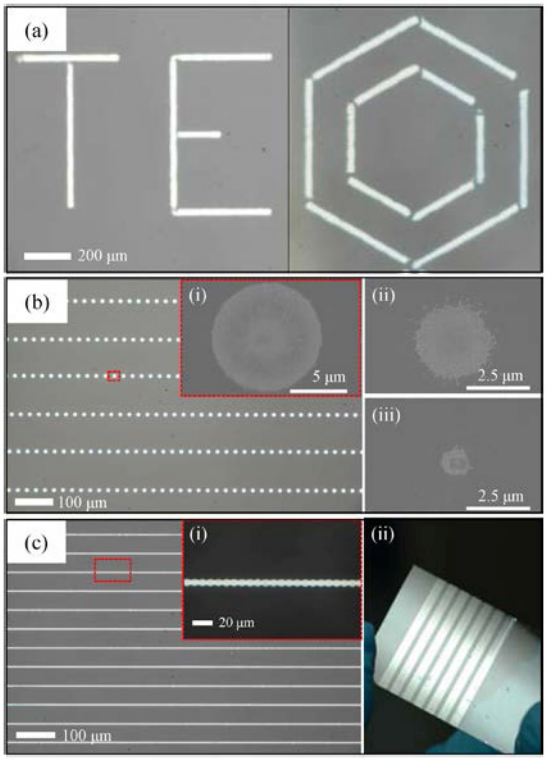

Fig. 4. (a) Arbitrary continuous pattern fabricated at a laser spot size of 25 μm, a pulse width of 14 ns, a pulse energy of 30 μJ, a scanning rate of 170 mm/s and a pulse repetition rate (PRR) of 7.5 kHz. (b) Microscope and SEM images of self-patterned dot patterns with a pulse energy of (i) 2 μJ, (ii) 1 μJ and (iii) 0.7 μJ at a spot size of 10 μm. (c) Microscope and photograph of self-patterned line patterns at a pulse energy of 1 μJ, a pulse width of 14 ns, PRR of 20 kHz and a scan rate of 170 mm/s.

This method can be characterized by varying process conditions. A pattern type could be readily changed from a disconnected dot pattern to continuous line pattern by properly reducing a feed per pulse ($F_p = \nu/R_p$) under adjusting either a laser scan rate (ν) or PRR (R_p). In addition, it was easy to change a pattern design by only modifying CAD data as a digital process, as shown in Fig. 4(a). The pattern resolution of this method could be further improved by decreasing the laser spot size with a tighter focusing optic system. As shown in Figs. 4(b)-4(i), the Ag dot patterns of approximately 10 μm could be fabricated by using a laser spot of 10 μm at a pulse energy of 2 μJ, a pulse width of 14 ns, PRR of 7 kHz and a scan rate of 170 mm/s. The deposited dot size decreased with decreasing the pulse energy below 2 μJ under a fixed laser spot (Figs. 4(b)-4(ii)). Finally, the Ag dot pattern of 850 nm, 11 times improved resolution than the laser spot as well as smaller size than the used laser wavelength, could be deposited selectively at a pulse energy of 0.7 μJ, as shown in Figs. 4(b)-4(iii). If the smaller laser spot than 10 μm is employed, although the spot size was constrained by the focusing limit of the used f-theta lens in this study, various nanopatterns could be realized with overcoming light diffraction limit. This phenomenon comes from that energy diffusion to surrounding area was suppressed in this method because very thin SAM (1~2 nm) was instantaneously deactivated by the bombardment of the energetic species in the plasma for very short time of tens nanosecond.

#175246 - $15.00 USD Received 30 Aug 2012; revised 5 Oct 2012; accepted 16 Oct 2012; published 14 Dec 2012

In the result of continuous pattern fabrication, the achievable minimum line width of 5 μm was recorded at a pulse energy of 1 μJ, a pulse width of 14 ns, PRR of 24 kHz and a scan rate of 170 mm/s, as shown in Fig. 4(c). The relative decline of the resolution in the continuous pattern compared to the disconnected one is because the treated SAM region was spatially broadened by the plasma re-exposure of the pre-processed region due to the spatial overlap of laser pulse train. In addition, it was observed that the edge of continuous line pattern was ribbed in the condition of 24 kHz PRR, as shown the inset of Fig. 4(c). If the PRR more increased than this PRR condition in order to straighten the pattern edge, the line pattern was disconnected irregularly and the pattern width was not uniform. Typically, the lateral area of Au layer ejected by a laser pulse is broader than that of plasma treated SAM region. It is considered that this is due to the strong cohesive force and high thermal conductivity of a vacuum deposited Au layer [26]. This is well-known phenomenon in the ns-pulse laser ablation of thin film. In this case, the uniform plasma could not be continuously generated by the subsequential pulse irradiations because the support of metal layer is not enough to induce the plasma, especially if the pulses are spatially overlapped less than laser spot. Therefore, it was concluded that the PRR should be controlled properly to obtain continuous line patterns considering the laser spot size and plasma treated area because the excessive spatial overlap of laser pulses induces the irregular plasma formation.

As a mass fabrication method, the pattern uniformity for large area and repeatability are also critical factors in the industry field. First, the pattern uniformity depended dominantly on the thickness uniformity of the vacuum deposited Au layer over the whole processing surface since the energy state of generated plasma could be affected by the thickness of target material. As a result, it was observed that the size of self-selectively deposited Ag NP solution tended to changed locally with the thickness variation of Au layer and the size variation was sensitive with decreasing laser pulse energy for improving the resolution. If, therefore, either the improved e-beam deposition instrument or sputter deposition is employed to deposit the Au layer more uniformly, the pattern uniformity for large area could be improved. In the same vein, the repeatability also depends on the repeatability of Au thickness every time it is deposited by e-beam evaporation, under the assumption that the material properties of Ag NP solution were not changed by solvents evaporation.

The self-patterned Ag NP solution represents an electrical property through a thermal sintering process. After the Ag solution-deposited glass was baked on a hot plate of 230 °C for 20 min as a sintering step, a resistivity of 2.94 μΩ·cm was recorded by using 4 probe resistance measurement. Although this value is still about 1.8 times higher than that of bulk Ag (1.6 μΩ·cm), it is noteworthy that this resistivity value is almost 2~3 times lower than that reported in the previous work using LDC methods [3,27]. Moreover, unlikely the limit of maximum thickness (~200 nm) by laser penetration depth in LDC [3,27], the thickness can be easily increased by adding the number of dip-coating times due to the hydrophilic characteristic of the pre-formed Ag film surface with own high surface energy [28,29]. As a method to improve the wettabilty of Ag NP solution on pre-formed Ag NP layer, the pre-deposited Ag NP solution was baked on a hot plate of 150 °C for 10 min as a pre-baking step. According to the thermal behavior of Ag NPs solution by thermogravimetry analysis (TGA) measurement shown in Fig. 5(a), most residual organic solvents in Ag NP solution was evaporated without the agglomeration of NPs. Because NPs were not aggregated each other in this low temperature, the microscopic contact area with post-deposited Ag solution more increased compared to the fully sintered Ag NP layer, as shown the inset of Fig. 5(a). The pre-baked specimen was additionally immersed in the solution. It was observed that the Ag solution was self-selectively deposited only on the pre-deposited Ag film in the same manner. The tendency of thickness variation was investigated with the number of dip-coating times. The thickness almost linearly increased from 150 nm to 980 nm with increasing the number of dip-coating times from 1 to 9, as shown in Fig. 5(b). Although the thickness was varied discretely with dip-coating times in this experiment, the pattern thickness will be controlled more finely by applying an additional diluted solution at a final dip-coating step. Therefore,

#175246 - $15.00 USD Received 30 Aug 2012; revised 5 Oct 2012; accepted 16 Oct 2012; published 14 Dec 2012

this result implied that this method has good controllability even in the aspect of thickness. And, of course, it is possible to obtain thicker pattern than 1 μm through repeating a series of this procedure. Figure 5(c) shows that cross-sectional SEM image of fabricated pattern after repeating the re-coating process of 50 times. The achievable maximum thickness approximately 6.6 μm was recorded, as shown the inset of Fig. 5(c). The cross-sectional profile appears a water droplet formed on a surface. The solution droplet placed on the defunctionalized surface retains a hemispherical shape with a high contact angle, as shown in Fig. 2(b). The presence of thicker liquid layer at the contact line of the droplet permits uniform slow evaporation to occur throughout the liquid/gas interface. In such a case, the contact line is retracts as the droplet shrinks while maintaining a hemispherical shape [30]. The more the number of coating increase, the more the hemispherical profile is remarkable due to the gradual concentration of Ag NP in center. This result is notable because this method can easily realize the much thicker pattern than 1 μm while creating the thick pattern above 1 μm using the conventional ink-jet and roll printing processes of the low viscosity NP solution is challenged due to alignment problems occurred during repeatedly overlaying the solution. Hereby, it is shown that this method can cover the fabrication from thin pattern of 100 nm to thick one of several micrometers with high conductivity and quality without using any expensive templates, chemical etching processes, and complicate fabrication steps.

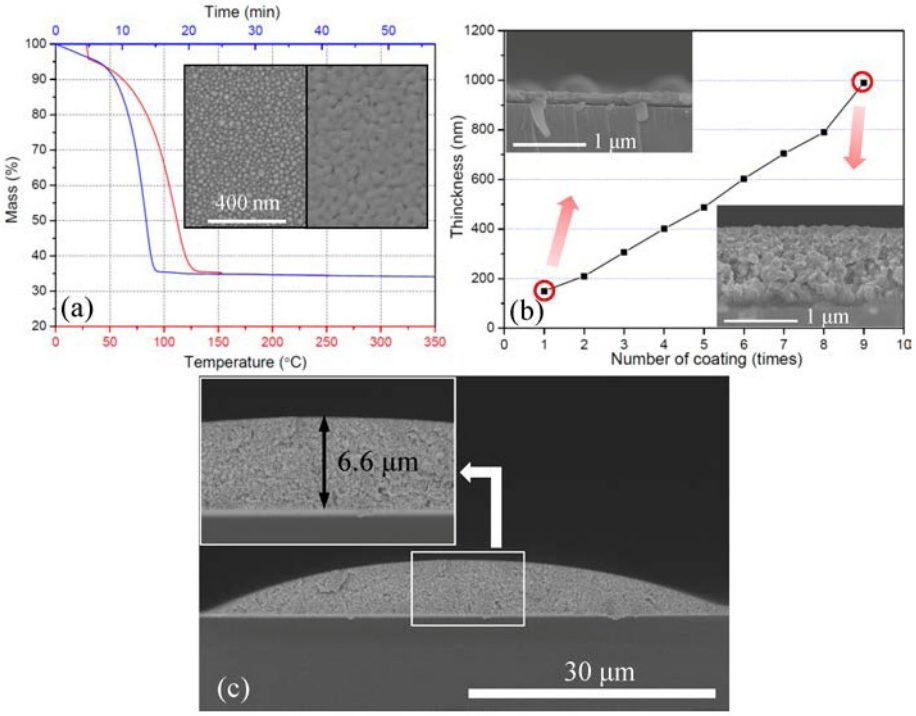

Fig. 5. (a) Thermogravimetry analysis (TGA) of the prepared Ag nanoparticle solution. The inset is SEM images of (i) pre-baked Ag NPs and (ii) sintered one. (b) Thickness variation of self-deposited pattern with immersing time and cross sectional SEM images of pattern at one and nine times immersing. (c) Cross-sectional SEM image of Ag pattern after the re-coating process of 50 times.

4. Conclusion

We have demonstrated a solution processable parallel self-patterning method based on laser induced plasmonic local defuctionalization of SAM as an adaptive mass fabrication method of high resolution pattern. The generation of laser induced local plasma and interaction with

#175246 - $15.00 USD Received 30 Aug 2012; revised 5 Oct 2012; accepted 16 Oct 2012; published 14 Dec 2012

SAM were optimized by the laser pulse width to prevent thermal damage of substrate and obtain high selectivity of self-patterned Ag solution. It was verified that the resolution, shape, type, and thickness was widely changeable in this method. Compared to the photolithography and other maskless techniques, although this method requires a laser patterning step, the productivity and resolution could be improved remarkably because it is possible to directly fabricate various patterns less than an optical focusing limit without any intermediate polymer patterning steps for etching, expensive templates, multiple vacuum processes and chemical etching process. In addition, the design can be changed more easily than that of lithography based on templates and the low-cost eco-friendly process is realizable due to the waste-free material deposition and disuse of harmful etchants.

Acknowledgments

This research was supported by Basic Science Research Program through the National Research Foundation of Korea (NRF) funded by the Ministry of Education, Science and Technology (No. 2012R1A2A1A01010307)

#175246 - $15.00 USD Received 30 Aug 2012; revised 5 Oct 2012; accepted 16 Oct 2012; published 14 Dec 2012